New Single-Source Surface Integral Equations for Scattering on Penetrable Cylinders and Current Flow Modeling in 2-D Conductors

Anton Menshov, *Student Member, IEEE*, and Vladimir Okhmatovski, *Senior Member, IEEE*

***Abstract*—The traditional volume electric field integral equation (IE) used for solution of full-wave scattering problems on penetrable scatterers of arbitrary cross section and its magnetostatic counterpart commonly utilized for the resistance and inductance extraction problem are reduced to a novel derivative-free single-source surface IE. The reduction of volume to surface IE is based on representation of the electric field in the cylinder cross section in the form of a single-layer ansatz. Substitution of such surface based electric field representation into the volume IE reduces it to a surface IE with respect to the unknown surface current density. Since the new surface IE enforces exactly the field continuity at the material interfaces, the radiation condition as well as underlying Helmholtz equations both inside and outside the penetrable cylinder, it is rigorously equivalent to the solution of Maxwell's equations. The method of moments discretization of the new IE is shown to produce an error-controllable field approximation. Due to the presence of a product of surface-to-volume and volume-to-surface integral operators, the discretization of the novel surface-volume-surface IE requires both surface and volume meshes.**

***Index Terms*—Boundary element method (BEM), computational electromagnetic (EM), EM theory, parameter extraction, scattering problems.**

I. Introduction

THE VOLUME electric field integral equation (V-EFIE) [1] has been widely used in computational electromagnetics for the rigorous solution of the Maxwell's equations in both quasi-static and full-wave regimes. Under quasi-static approximation, the V-EFIE is foundational to the evaluation of the current distribution in the cross sections of 2-D [2] as well as 3-D conductors [3]. Such solutions have an important practical application in the extraction of per-unit-length (p.u.l.) and terminal characteristics of the multiconductor transmission lines (MTLs) [4]. In the full-wave regime, the V-EFIE is most commonly used for solution of the scattering problems on penetrable scatterers with inhomogeneous distribution of permittivity and/or conductivity [1]. Such problems are commonly encountered in microwave imaging [5], remote sensing [6], design of radar absorber materials [7], [8], and various other areas.

The use of the V-EFIE may be avoided, however, when the scatterer is homogeneous or partially homogeneous. In these situations, it is common to utilize the surface integral equations (IEs) instead [9], [10]. The main benefit of surface IE formulations compared to the V-EFIE is in confinement of the unknown field quantities to the boundaries of material interfaces, the property which greatly reduces the computational complexity associated with their numerical solution. For the purpose of discussion in this paper, however, its important to note that the traditional surface IEs [9], [10] have two unknown functions, tangential electric and magnetic fields, on the boundary of material domains with different physical parameters. These surface IEs also feature first- and/or second-order derivatives acting on their kernels. In the quest to further reduce the computational complexity, alternative single-source surface integral equation (SSIE) formulations have also been introduced [11]–[16] that utilize only a single unknown current density at the material boundaries. These formulations though come at a price of having a large number of independent kernels, as well as their products rendering the numerical solutions difficult. Due to this large number of operator products, the SSIEs may produce higher computational complexity compared with the standard Muller or Poggio, Miller, Chang, Harrington, Wu, and Tsai (PMCHWT) equations despite the latter having two unknown surface currents.

To further simplify evaluation of electromagnetic fields in the presence of penetrable objects, in this work we propose an alternative SSIE. The new formulation features a single unknown current density similar to other SSIEs [11]–[16], but has only a single product of integral operators. These operators also have additional advantage of being derivative free. The absence of the derivative comes as an important property if the kernels are available only through a numerical evaluation procedure as, for example, in the case of multilayered media [1]. Such derivatives act as amplifiers of the numerical error, and their presence greatly increases the accuracy requirements on the evaluation of already computationally demanding Sommerfeld integrals [1], [22].

In the derivation of the new surface IE, we start from the traditional V-EFIE. Assuming the material properties of the scatterer homogeneous, we can represent the electric field at any point inside the scatter as a superposition of the elementary cylindrical waves emanating from the scatterer's boundary. Such electric field representation is in the form of the surface integral of the

Manuscript received July 10, 2012; revised October 05, 2012; accepted October 15, 2012. Date of publication December 12, 2012; date of current version January 17, 2013.This work was supported by Manitoba Hydro under Research Grant T311. This paper is an expanded paper from the IEEE MTT-S International Microwave Symposium, Montreal, QC, Canada, June 17–22, 2012.

The authors are with the Department of Electrical and Computer Engineering, University of Manitoba, Winnipeg, MB, Canada R3T 5V6 (e-mail: anton_menshov@umanitoba.ca; okhmatov@cc.umanitoba.ca).

Color versions of one or more of the figures in this paper are available online at http://ieeexplore.ieee.org.

Digital Object Identifier 10.1109/TMTT.2012.2227784

product of a surface current density multiplied with the Green's function also known as single-layer ansatz [17], which is different from that of the traditional field representation via the equivalence principle [18]. In the latter, both tangential electric and magnetic fields participate in the formation of the electric field. In the single-layer ansatz representation of the field, however, the surface current density has no apparent relationship to either electric and magnetic field on the surface. It has the meaning of merely being a weighting function for the elementary waves emanating from the surface and each satisfying the Helmholtz equation inside the scatterer. This single-source representation of the field upon substitution of the V-EFIE followed by the restriction of its observation domain to the scatterer's surface reduces the V-EFIE to an SSIE. Due to the nature of field translations in the resultant IE, we further term it as the surface–volume–surface electric field integral equation (SVS-EFIE). The approach described above has proven to be applicable for both the problems of magneto-quasi-statics [19], [20], as well as to the full-wave problems of scattering on penetrable objects. The latter applications are originally described in this paper and constitute a major extension to our prior work published in [19] and [20].

II. Novel Single-Source SVS-EFIE Formulation

A. Magnetostatics Formulation

The electric field $\boldsymbol{E} = \hat{\boldsymbol{z}}E_z$ inside a 2-D conductor of arbitrary cross section S having invariant bulk conductivity σ along the coordinate z and linear variation of electrostatic potential ϕ along the same coordinate is governed by the following V-EFIE of magneto-quasi-statics [2], [3]:

$$E_z(\boldsymbol{\rho}) + i\omega\mu_0\sigma \iint_S G_0^{qs}(\boldsymbol{\rho},\boldsymbol{\rho}')E_z(\boldsymbol{\rho}')\,ds' = -\frac{d\phi}{dz}, \boldsymbol{\rho} \in S \quad (1)$$

where ω is the cyclic frequency, $i = \sqrt{-1}$, $\boldsymbol{\rho}$, and $\boldsymbol{\rho}'$ are the observation and source points in the conductor's cross section, respectively, $G_0^{qs}(\boldsymbol{\rho},\boldsymbol{\rho}') = -(1)/(2\pi)\ln(|\boldsymbol{\rho}-\boldsymbol{\rho}'|)$ is the 2-D Green's function of the vacuum exterior to the conductor $-(i/4)H_0^{(2)}(k_0|\boldsymbol{\rho}-\boldsymbol{\rho}'|)$ under quasi-static assumption $k_0|\boldsymbol{\rho}-\boldsymbol{\rho}'| \ll 1$, μ_0, ε_0, and $k_0 = \omega\sqrt{\mu_0\varepsilon_0}$ are the permeability, permittivity, and wavenumber of vacuum, respectively. The constant derivative of linearly varying scalar potential with respect to the coordinate z in the right-hand side of the V-EFIE (1) is commonly termed as p.u.l. voltage drop [4] along the wire $V_{\text{p.u.l.}} = -(d\phi)/(dz)$.

Assuming the bulk conductivity σ homogeneous throughout the conductor cross section and taking into consideration the fact that the electric field E_z inside the conductor satisfies the homogeneous Helmholtz equation,

$$\nabla^2 E_z(\boldsymbol{\rho}) + k_\sigma^2 E_z(\boldsymbol{\rho}) = 0, \boldsymbol{\rho} \in S \quad (2)$$

we express the E-field in the conductor cross section as a superposition of cylindrical waves emanating from its boundary

$$E_z(\boldsymbol{\rho}) = -i\omega\mu_0 \int_{\partial S} G_\sigma(\boldsymbol{\rho},\boldsymbol{\rho}')J_z(\boldsymbol{\rho}')\,d\boldsymbol{\rho}', \boldsymbol{\rho} \in S. \quad (3)$$

In (3), $J_z(\boldsymbol{\rho}')$ is an auxiliary surface current density that plays a role of a weighting function for the elementary cylindrical waves $G_\sigma(\boldsymbol{\rho},\boldsymbol{\rho}') = -(i/4)H_0^{(2)}(k_\sigma|\boldsymbol{\rho}-\boldsymbol{\rho}'|)$ emanating from the surface S, $H_0^{(2)}$ is the second-kind Hankel function of zeroth order [21]. The latter satisfies the Helmholtz equation

$$\nabla^2 G_\sigma(\boldsymbol{\rho},\boldsymbol{\rho}') + k_\sigma^2 G_\sigma(\boldsymbol{\rho},\boldsymbol{\rho}') = 0 \quad (4)$$

at the points in the cross section S excluding the boundary ∂S containing the source points $\boldsymbol{\rho}'$. In (2)–(4), $k_\sigma = -i\sqrt{i\omega\mu_0\sigma}$ is the wavenumber of the conductor material. It is important to note that the integral field representation (3), called single layer ansatz [17], is different from that of the standard equivalence principle

$$E_z(\boldsymbol{\rho}) = i\omega\mu_\sigma \int_{\partial S} G_\sigma(\boldsymbol{\rho},\boldsymbol{\rho}')J_z^e(\boldsymbol{\rho}')d\boldsymbol{\rho}' + \int_{\partial S} \frac{\partial G_\sigma(\boldsymbol{\rho},\boldsymbol{\rho}')}{\partial n} J_t^m(\boldsymbol{\rho}')d\boldsymbol{\rho}', \boldsymbol{\rho} \in S. \quad (5)$$

The field representation (5) utilizes both equivalent electric current density J_z^e and magnetic current density J_t^m for the field representation inside the conductor. In subsequent discussion of the numerical results, the auxiliary surface current density J_z in (3) is depicted against the electric and magnetic current densities J_z^e and J_t^m for TM_z wave scattering from a single dielectric cylinder, showing that there is no apparent relationship between the auxiliary surface current density J_z and electric and magnetic field components J_z^e and J_t^m. It can also be shown that auxiliary surface current density J_z cannot be represented as a superposition of the equivalent electric current density J_z^e and magnetic current density J_t^m either.

Substitution of the (3) into (1) followed by the restriction of the observation domain to the conductor surface produces a SSIE with respect to the unknown auxiliary surface current density J_z as follows:

$$-i\omega\mu_0 \int_{\partial S} G_\sigma(\boldsymbol{\rho},\boldsymbol{\rho}')J_z(\boldsymbol{\rho}')\,d\boldsymbol{\rho}' - \sigma(\omega\mu_0)^2 \times \int_{\partial S} \left[\iint_S G_0^{qs}(\boldsymbol{\rho},\boldsymbol{\rho}')G_\sigma(\boldsymbol{\rho},\boldsymbol{\rho}'')\,ds'\right] J_z(\boldsymbol{\rho}'')d\boldsymbol{\rho}'' = -V_{\text{p.u.l.}}, \boldsymbol{\rho} \in \partial S. \quad (6)$$

Using the following notation for the integral operators entering in (6):

$$\mathcal{T}_{\sigma}^{\partial S,\partial S} \circ J_z = -i\omega\mu_0 \int_{\partial S} G_{\sigma}(\boldsymbol{\rho},\boldsymbol{\rho}') J_z(\boldsymbol{\rho}')\, d\boldsymbol{\rho}', \boldsymbol{\rho} \in \partial S \quad (7)$$

$$\mathcal{T}_{\sigma}^{S,\partial S} \circ J_z = -i\omega\mu_0 \int_{\partial S} G_{\sigma}(\boldsymbol{\rho},\boldsymbol{\rho}') J_z(\boldsymbol{\rho}')\, d\boldsymbol{\rho}', \boldsymbol{\rho} \in S \quad (8)$$

$$\mathcal{T}_{0}^{\partial S,S} \circ E_z = -i\omega\mu_0 \iint_{S} G_0^{qs}(\boldsymbol{\rho},\boldsymbol{\rho}') E_z(\boldsymbol{\rho}')\, ds', \boldsymbol{\rho} \in \partial S \quad (9)$$

we can rewrite IE (6) in the concise operator form as

$$\mathcal{T}_{\sigma}^{\partial S,\partial S} \circ J_z + \sigma \mathcal{T}_{0}^{\partial S,S} \circ \mathcal{T}_{\sigma}^{S,\partial S} \circ J_z = -V_{\text{p.u.l.}}. \quad (10)$$

The derived IE is termed the SVS-EFIE [19], [20] due to the nature of the field translation operations from the surface of conductor to its volume and subsequent translation of the field back to the surface as expressed by the product of integral operators $\mathcal{T}_{0}^{\partial S,S} \circ \mathcal{T}_{\sigma}^{S,\partial S}$. The SVS-EFIE is rigorous since it forces the field to satisfy the Helmholtz equations both inside and outside the conductor, as well as satisfies the continuity of tangential field components at the conductor boundary, which is inherent to the V-EFIE (1). The SVS-EFIE also comes with the benefit of being free of derivatives acting on the kernels. This property becomes important when conductor is situated in multilayered media for which the Green's function is only available through the numerical evaluation [1], [22] and the derivatives act as numerical noise amplifiers. The new IE (10) also contains only a single unknown surface function J_z as opposed to the traditional surface IEs based on the equivalence principle field representation (5) requiring two unknown functions J_z^e and J_t^m. These benefits, however, come at the price of having the conductor's volume as the intermediate range and domain in the product of the operators, which requires both volume and surface discretization in the MoM solution, as shown in Section III.

B. Full-Wave Formulation

Similar new single-source integral equation can be derived from the V-EFIE for full-wave scattering problems. Consider a 2-D TM-scattering problem for a dielectric cylinder directed along z-coordinate and having arbitrary cross section with area S. The V-EFIE in the electrodynamic case is written as [1], [23]

$$E_z(\boldsymbol{\rho}) - k_0^2(\epsilon - 1) \iint_{S} G_0(\boldsymbol{\rho},\boldsymbol{\rho}') E_z(\boldsymbol{\rho}')\, ds' = E_z^{\text{inc}}(\boldsymbol{\rho}), \boldsymbol{\rho} \in S \quad (11)$$

where E_z is the unknown distribution of the field inside the cylinder, $G_0(\boldsymbol{\rho},\boldsymbol{\rho}') = -(i/4)H_0^{(2)}(k_0|\boldsymbol{\rho} - \boldsymbol{\rho}'|)$ is the Green's function of free space, $\epsilon = \varepsilon + \sigma/(i\omega\varepsilon_0) = \varepsilon(1 - i\tan\delta)$ is the complex relative permittivity of the dielectric cylinder, and E_z^{inc} is the incident field impinging on the cylinder.

Similar to the magnetostatic case, we represent the distribution of the field inside the cylinder E_z satisfying the Helmholtz equation $\nabla^2 E_z + k_\epsilon^2 E_z = 0$ as a superposition of cylindrical waves emanating from the cylinder's surface and having the strength defined with the function $\mathtt{J}_z(\boldsymbol{\rho}')$ playing the role of an auxiliary surface current density

$$E_z(\boldsymbol{\rho}) = -i\omega\mu_0 \int_{\partial S} G_{\epsilon}(\boldsymbol{\rho},\boldsymbol{\rho}') \mathtt{J}_z(\boldsymbol{\rho}')\, d\boldsymbol{\rho}', \boldsymbol{\rho} \in S. \quad (12)$$

In (12), $G_\epsilon(\boldsymbol{\rho},\boldsymbol{\rho}') = -(i/4)H_0^{(2)}(k_\epsilon|\boldsymbol{\rho} - \boldsymbol{\rho}'|)$ is the Green's function of the dielectric media with the wavenumber $k_\epsilon = \omega\sqrt{\mu_0\varepsilon_0\epsilon}$ satisfying the Helmholtz equation $\nabla^2 G_\epsilon + k_\epsilon^2 G_\epsilon = 0$ everywhere in S excluding the boundary ∂S. Once again, we emphasize here that the weighted superposition of cylindrical waves (12) is different from the equivalence principle field representation in terms of the tangential field components on the boundary of the cylinder.

Substitution of (12) into (11) followed by the restriction of the observation domain to the conductor surface yields the desired SVS-EFIE with respect to the unknown current density

$$\begin{aligned} &- i\omega\mu_0 \int_{\partial S} G_{\epsilon}(\boldsymbol{\rho},\boldsymbol{\rho}') \mathtt{J}_z(\boldsymbol{\rho}')\, d\boldsymbol{\rho}' - i\omega\mu_0 k_0^2(\epsilon - 1) \\ &\quad \times \int_{\partial S} \left[\iint_{S} G_0(\boldsymbol{\rho},\boldsymbol{\rho}') G_{\epsilon}(\boldsymbol{\rho},\boldsymbol{\rho}'') ds' \right] \mathtt{J}_z(\boldsymbol{\rho}'') d\boldsymbol{\rho}'' \\ &\quad = E_z^{\text{inc}}(\boldsymbol{\rho}), \boldsymbol{\rho} \in \partial S. \end{aligned} \quad (13)$$

In the operator form, the above SVS-EFIE is expressed as follows:

$$\mathtt{T}_{\epsilon}^{\partial S,\partial S} \circ \mathtt{J}_z + \mathtt{T}_{0}^{\partial S,S} \circ \mathtt{T}_{\epsilon}^{S,\partial S} \circ \mathtt{J}_z = E_z^{\text{inc}} \quad (14)$$

where the integral operators are defined as

$$\mathtt{T}_{\epsilon}^{\partial S,\partial S} \circ \mathtt{J}_z = -i\omega\mu_0 \int_{\partial S} G_{\epsilon}(\boldsymbol{\rho},\boldsymbol{\rho}') \mathtt{J}_z(\boldsymbol{\rho}')\, d\boldsymbol{\rho}', \boldsymbol{\rho} \in \partial S \quad (15)$$

$$\mathtt{T}_{\epsilon}^{S,\partial S} \circ \mathtt{J}_z = -i\omega\mu_0 \int_{\partial S} G_{\epsilon}(\boldsymbol{\rho},\boldsymbol{\rho}') \mathtt{J}_z(\boldsymbol{\rho}')\, d\boldsymbol{\rho}', \boldsymbol{\rho} \in S \quad (16)$$

$$\mathtt{T}_{0}^{\partial S,S} \circ E_z = k_0^2(\epsilon - 1) \iint_{S} G_0(\boldsymbol{\rho},\boldsymbol{\rho}') E_z(\boldsymbol{\rho}')\, ds', \boldsymbol{\rho} \in \partial S. \quad (17)$$

III. Method of Moments (MoM) Discretization

The MoM discretization of the SVS-EFIE (6) for magneto-quasi-statics was discussed in detail in [20] for the case of a coaxial cable model featuring a multiconnected domain formed by the outer shell and a single-connected domain formed by the cable's inner conductor. In this paper, we present a similar detailed description of the MoM discretization for the case of the full-wave SVS-EFIE (13), (14) applied to the problem of TM_z wave scattering on a pair of dielectric cylinders of an arbitrary cross section depicted in Fig. 1.

The range of the integral operator $\mathtt{T}_{\epsilon}^{S,\partial S}$ in (16) mapping the auxiliary surface current density $\mathtt{J}_z$ to the volumetric polarization current $j_z = k_0^2(\epsilon - 1)E_z$ is on the cross section of the scatterers S_A and S_B. The same is true for the domain of the operator $\mathtt{T}_{0}^{\partial S,S}$ in (17), which maps the polarization current j_z to

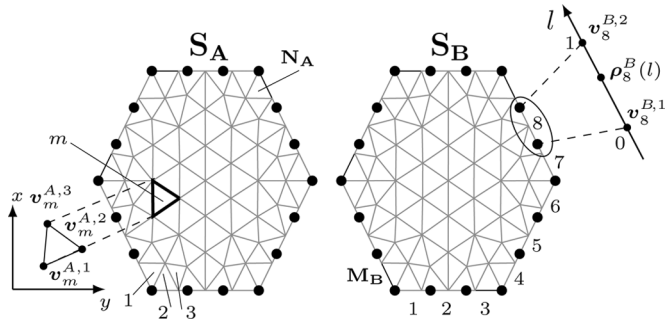

Fig. 1. Volume and surface meshes utilized in the MoM discretization of the SVS-EFIE (13).

the scattered electric field E_z^{scat}. These cross sections are therefore discretized with a volumetric mesh consisting of $N_A + N_B$ triangular elements. The surfaces of the scatterers ∂S_A and ∂S_B forming the ranges and domains of the remaining operators in the SVS-EFIE (13), (14) are discretized with M_A and M_B linear elements, respectively. Depiction of the combined volumetric and surface meshes is shown in Fig. 1.

It is important to mention here that while in our previous work [19], [20] the size of the volume and surface meshes were reported to be independent, our further studies have shown that choosing these meshes independently is suboptimal. To obtain the minimum error, the sizes of the surface and volume meshes must be related to both the frequency and each other. Quantitative description of the error dependence on the mesh sizes is presented in Section IV.

The radius-vector on mth straight element of the mesh discretizing surfaces ∂S_α is defined parametrically as

$$\boldsymbol{\rho}_m^\alpha(l) = \boldsymbol{v}_m^{\alpha,1} + l\left(\boldsymbol{v}_m^{\alpha,2} - \boldsymbol{v}_m^{\alpha,1}\right), \qquad l \in [0,1]; \quad \alpha = A, B \tag{18}$$

where $\boldsymbol{v}_m^{\alpha,2}$ and $\boldsymbol{v}_m^{\alpha,1}$ are the vertices of mth element on ∂S_α, L_m^α is its length $|\boldsymbol{v}_m^{\alpha,2} - \boldsymbol{v}_m^{\alpha,1}|$, and $m = 1, \ldots, M_\alpha$.

Similarly, the position-vector on mth triangular element of the cross section S_β is defined parametrically in the barycentric coordinates [18] as

$$\boldsymbol{\rho}_m^\beta(\xi,\eta) = \boldsymbol{v}_m^{\beta,1}\xi + \boldsymbol{v}_m^{\beta,2}\eta + \boldsymbol{v}_m^{\beta,3}(1-\xi-\eta), \quad \xi,\eta \in [0,1] \tag{19}$$

where $\xi + \eta \le 1$, $\beta = A, B$ is the scatterer's label, $\boldsymbol{v}_m^{\beta,1}$, $\boldsymbol{v}_m^{\beta,2}$, $\boldsymbol{v}_m^{\beta,3}$ are the mth element vertices, and $m = 1, \ldots, N_\beta$.

A. MoM Discretization of SVS-EFIE's Surface-to-Volume Operator $\mathtt{T}_\epsilon^{S,\partial S}$

Discretization of the unknown surface current densities $\mathtt{J}_z^A$ and $\mathtt{J}_z^B$ on the scatterer's sub-surfaces ∂S_A and ∂S_B is performed using the piece-wise basis functions [24]

$$\mathtt{J}^\alpha(\boldsymbol{\rho}'') \cong \sum_{m=1}^{M_\alpha} I_m^\alpha P_m^\alpha(\boldsymbol{\rho}'')$$
$$P_m^\alpha(\boldsymbol{\rho}'') = \begin{cases} 1, & \boldsymbol{\rho}'' \in \partial S_{\alpha,m} \\ 0, & \boldsymbol{\rho}'', \notin \partial S_{\alpha,m} \end{cases} \tag{20}$$

with $\alpha = A, B$ being the sub-surface label, and $\partial S_{\alpha,m}$ denoting the mth surface mesh element on ∂S_α. In (20) and throughout this section, the subscript z denoting the component of the currents and fields is omitted for brevity. As testing functions, we use delta-functions positioned at the centroid of the volumetric mesh triangles

$$t_{n'}^\beta(\boldsymbol{\rho}) = \delta\left(\boldsymbol{\rho} - \boldsymbol{\rho}_{n'}^\beta\left(\frac{1}{3},\frac{1}{3}\right)\right). \tag{21}$$

In (21), $\boldsymbol{\rho}_{n'}^\beta((1/3),(1/3))$ is the radius-vector to the centroid of the n'th volume element in S_β cross section.

Substitution of (20) into the operator relation $j = \mathtt{T}_\epsilon^{S,\partial S} \circ \mathtt{J}$ in (16) followed by the point-sampling of polarization current j in its range with test functions (21) casts (16) into the following matrix form:

$$\begin{bmatrix} \mathbf{i}^A \\ \mathbf{i}^B \end{bmatrix} = \begin{bmatrix} \mathbf{Z}_\epsilon^{S_A,\partial S_A} & 0 \\ 0 & \mathbf{Z}_\epsilon^{S_B,\partial S_B} \end{bmatrix} \cdot \begin{bmatrix} \mathbf{I}^A \\ \mathbf{I}^B \end{bmatrix}. \tag{22}$$

In (22), $\mathbf{I} = [I_1^A, \ldots, I_{M_A}^A; I_1^B, \ldots, I_{M_B}^B]^T$ is the vector of unknown current expansion coefficients in (20), and vector $\mathbf{i} = [i_1^A, \ldots, i_{N_A}^A; i_1^B, \ldots, i_{N_B}^B]^T$ contains the N values of polarization current j at the $N_A + N_B$ centroids of the triangle mesh elements discretizing cross section of the scatterers S_A and S_B. The matrix elements in (22) are the inner products [24]

$$\begin{aligned} Z_{\epsilon,n'm''}^{S_\beta,\partial S_\alpha} &= \left\langle t_{n'}^\beta, \mathtt{T}_\epsilon^{S_\beta,\partial S_\alpha} \circ P_{m''}^\alpha \right\rangle \\ &= -i\omega\mu_0 L_{m''}^\alpha \int_0^1 G_\epsilon\left(\boldsymbol{\rho}_{n'}^\beta\left(\frac{1}{3},\frac{1}{3}\right), \boldsymbol{\rho}_{m''}^\alpha(l'')\right) dl'' \end{aligned} \tag{23}$$

where $n' = 1, \ldots, N_\alpha$ are the indices of the surface elements on ∂S_α, and $m'' = 1, \ldots, M_\beta$ are the indices of the volume elements in S_β. Parametric definitions of position-vectors on the surface and volume elements in (23) are given in (18) and (19), respectively.

The evaluation of line integrals in (23) can be done to desired precision using standard Gauss-Legendre Q-point quadrature rules [25] with weights w_q and abscissas l_q, $q = 1, \ldots, Q$, applied to the integrand after its singular part $-(1)/(2\pi)\ln|\boldsymbol{\rho} - \boldsymbol{\rho}'|$ has been extracted

$$\begin{aligned} &Z_{\epsilon,n'm''}^{S_\beta,\partial S_\alpha} \\ &\quad = i\omega\mu_0 L_{m''}^\alpha \\ &\qquad \times \int_0^1 \frac{\ln\left|\boldsymbol{\rho}_{n'}^\beta\left(\frac{1}{3},\frac{1}{3}\right) - \boldsymbol{\rho}_{m''}^\alpha(l'')\right|}{2\pi} dl'' - i\omega\mu_0 L_{m''}^\alpha \sum_{q=1}^{Q} w_q \\ &\qquad \times \left[G_\epsilon\left(\boldsymbol{\rho}_{n'}^\beta\left(\frac{1}{3},\frac{1}{3}\right), \boldsymbol{\rho}_{m''}^\alpha(l_q'')\right) \right. \\ &\qquad\quad \left. + \frac{\ln\left|\boldsymbol{\rho}_{n'}^\beta\left(\frac{1}{3},\frac{1}{3}\right) - \boldsymbol{\rho}_{m''}^\alpha(l_q'')\right|}{2\pi} \right]. \end{aligned} \tag{24}$$

The integral of logarithmic function over a linear element can be evaluated analytically for an arbitrary observation point location using the technique in [26].

B. MoM Discretization of SVS-EFIE's Volume-to-Surface Operator $\mathtt{T}_0^{\partial S,S}$

Discretization of the domain of the volume-to-surface integral operator $\mathtt{T}_0^{\partial S,S}$ in (17), which maps the volumetric polarization current density $j = k_0^2(\epsilon - 1)E$ inside the scatterer volume S to the scattered electric field $E^{\text{scat}} = -i\omega\mu_0 \int_S G_0 j ds'$ on scatterer's surface ∂S, is performed using pulse basis functions [10], [24] defined on the volumetric mesh

$$j^\beta(\boldsymbol{\rho}') \cong \sum_{n=1}^{N_\beta} i_n^\beta p_n^\beta(\boldsymbol{\rho}')$$
$$p_n^\beta(\boldsymbol{\rho}') = \begin{cases} 1, & \boldsymbol{\rho}' \in S_{\beta,n} \\ 0, & \boldsymbol{\rho}' \notin S_{\beta,n} \end{cases} \tag{25}$$

where $S_{\beta,n}$, $n = 1, \ldots, N_\beta$ are the volumetric mesh elements and $\beta = A, B$ is the index identifying the sub-volume S_β of the scatterer's cross section. The range of the $\mathtt{T}_0^{\partial S,S}$ operator is tested with delta-functions [10], [24]

$$T_m^\alpha(\boldsymbol{\rho}) = \delta\left(\boldsymbol{\rho} - \boldsymbol{\rho}_m^\alpha\left(\frac{1}{2}\right)\right) \tag{26}$$

positioned at the centroids of mth elements in the surface discretization of the scatterer's boundary ∂S_α. Here, α is the index of a sub-scatterer ∂S_α, and $m = 1, \ldots, M_\alpha$ are the indices of the surface elements in ∂S_α.

Substitution of the volume polarization current j expansion (25) into its integral relation to the scattered field $E^{\text{scat}} = \mathtt{T}_0^{\partial S,S} \circ j$ in (17) produces the following matrix relationship:

$$\begin{bmatrix} \mathbf{E}^{\text{scat},A} \\ \mathbf{E}^{\text{scat},B} \end{bmatrix} = \begin{bmatrix} \mathbf{Z}_0^{\partial S_A,S_A} & \mathbf{Z}_0^{\partial S_A,S_B} \\ \mathbf{Z}_0^{\partial S_B,S_A} & \mathbf{Z}_0^{\partial S_B,S_B} \end{bmatrix} \cdot \begin{bmatrix} \mathbf{i}^A \\ \mathbf{i}^B \end{bmatrix} \tag{27}$$

where $\mathbf{E}^{\text{scat}} = [E_1^{\text{scat},A}, \ldots, E_{M_A}^{\text{scat},A}; E_1^{\text{scat},B}, \ldots, E_{M_B}^{\text{scat},B}]^T$ is a vector of M samples of the scattered electric field E^{scat} produced at the centroids of the surface mesh elements by the polarization current j, and the matrix elements in (27) are defined as the inner products

$$\begin{aligned} Z_{0,mn'}^{\partial S_\alpha,S_\beta} &= \left\langle T_m^\alpha, \mathtt{T}_0^{\partial S_\alpha,S_\beta} \circ p_{n'}^\alpha \right\rangle \\ &= -i\omega\mu_0 2A_{n'}^\beta \int_0^1 \int_0^{1-\eta'} G_0\left(\boldsymbol{\rho}_m^\alpha\left(\frac{1}{2}\right), \boldsymbol{\rho}_{n'}^\beta(\xi', \eta')\right) d\xi' d\eta'. \end{aligned} \tag{28}$$

In order to match discretized range of $\mathtt{T}_\epsilon^{S,\partial S}$ (16), which is sampled with the test delta-functions (21) to the discretized domain of $\mathtt{T}_0^{\partial S,S}$ (17) expanded over piece-wise basis functions (25), the integral over triangular area is approximated with the one-point quadrature rule as follows:

$$Z_{0,mn'}^{\partial S_\alpha,S_\beta} \cong -i\omega\mu_0 A_{n'}^\beta G_0\left[\boldsymbol{\rho}_m^\alpha\left(\frac{1}{2}\right), \boldsymbol{\rho}_{n'}^\beta(1/3, 1/3)\right]. \tag{29}$$

We note that the adopted discretization procedure chosen here for the domain of operator $\mathtt{T}_0^{S,\partial S}$ can be viewed as taking delta-functions as the basis functions (25) instead of taking the piece-wise basis functions and selecting the single-point integration quadrature over the volume elements. Alternative choices for the basis and testing functions are also possible [10], [24]. In the general case, however, when the domain of $\mathtt{T}_0^{\partial S,S}$ is expanded over a different basis than the range of the operator $\mathtt{T}_\epsilon^{S,\partial S}$, the product of operators $\mathtt{T}_0^{\partial S,S} \circ \mathtt{T}_\epsilon^{S,\partial S}$ requires the appropriate Gramian matrix [27] affecting the conversion of spaces spanning the domain of $\mathtt{T}_0^{\partial S,S}$ and the range of $\mathtt{T}_\epsilon^{S,\partial S}$.

C. MoM Discretization of SVS-EFIE's Surface-to-Surface Operator $\mathtt{T}_\epsilon^{\partial S,\partial S}$

The representation of the electric field inside the scatterer as a superposition of cylindrical waves (12) has the form of a global surface impedance operator $\mathtt{T}_\epsilon^{\partial S,\partial S}$ relating the auxiliary surface current density $\mathtt{J}$ to the electric field E as formalized by (15). Both domain and range of $\mathtt{T}_\epsilon^{\partial S,\partial S}$ are at the scatterer's surface ∂S. Discretizing the domain of $\mathtt{T}_\epsilon^{\partial S,\partial S}$ over piece-wise basis functions as in (20) and testing the total electric field in its range with the delta-functions (26), we cast the surface impedance operator into a matrix form

$$\begin{bmatrix} \mathbf{E}^A \\ \mathbf{E}^B \end{bmatrix} = \begin{bmatrix} \mathbf{Z}_\epsilon^{\partial S_A,\partial S_A} & 0 \\ 0 & \mathbf{Z}_\epsilon^{\partial S_B,\partial S_B} \end{bmatrix} \cdot \begin{bmatrix} \mathbf{I}^A \\ \mathbf{I}^B \end{bmatrix}. \tag{30}$$

In (30), vector $\mathbf{E} = [E_1^A, \ldots, E_{M_A}^A; E_1^B, \ldots, E_{M_B}^B]^T$ contains M samples of the electric field E at the centroids of the surface mesh elements on the scatterer's surface ∂S, and the inner products defining the matrix elements in (30) are

$$\begin{aligned} Z_{\epsilon,mm'}^{\partial S_\alpha,\partial S_{\alpha'}} &= \left\langle T_m^\alpha, \mathtt{T}_\epsilon^{\partial S,\partial S} \circ P_{m'}^{\alpha'} \right\rangle \\ &= -i\omega\mu_0 L_{m'}^{\alpha'} \int_0^1 G_\epsilon\left(\boldsymbol{\rho}_m^\alpha\left(\frac{1}{2}\right), \boldsymbol{\rho}_{m'}^{\alpha'}(l')\right) dl', \end{aligned} \tag{31}$$

where $\alpha, \alpha' = A, B$ are indices of scatterer's sub-surfaces, $m = 1, \ldots M_\alpha$, and $m' = 1, \ldots, M_{\alpha'}$. The singular integrals in (31) are handled via singularity extraction similar to (24)

$$\begin{aligned} Z_{\epsilon,mm'}^{\partial S_\alpha,\partial S_{\alpha'}} &= i\omega\mu_0 L_{m'}^{\alpha'} \\ &\times \int_0^1 \frac{\ln\left|\boldsymbol{\rho}_m^\alpha\left(\frac{1}{2}\right) - \boldsymbol{\rho}_{m'}^{\alpha'}(l')\right|}{2\pi} dl' - i\omega\mu_0 L_{m'}^{\alpha'} \sum_{q=1}^{Q} w_q \\ &\times \left[G_\epsilon\left(\boldsymbol{\rho}_m^\alpha\left(\frac{1}{2}\right), \boldsymbol{\rho}_{m'}^\alpha(l_q')\right) + \frac{\ln\left|\boldsymbol{\rho}_m^\alpha\left(\frac{1}{2}\right) - \boldsymbol{\rho}_{m'}^{\alpha'}(l_q')\right|}{2\pi}\right]. \end{aligned} \tag{32}$$

Alternatively, the singular integrals can be handled using specially developed quadrature rules [28].

TABLE I
COMPUTATIONAL COMPLEXITY COMPARISON FOR DIRECT AND ITERATIVE SOLUTION OF THE V-EFIE (11), SVS-EFIE (13), AND PMCHWT [10] EQUATIONS

	V-EFIE	SVS-EFIE	PMCHWT
Matrix Fill	$\mathbf{Z}^{\mathbf{S},\mathbf{S}}$	$\mathbf{Z}^{\mathbf{S},\partial\mathbf{S}}$, $\mathbf{Z}^{\partial\mathbf{S},\mathbf{S}}$	$\mathbf{Z}^{\partial\mathbf{S},\partial\mathbf{S}}$
LU [25]	$O(M^4)$	$O(M^3)+O(M^4)$	$O(M^2)$
Iterative (e.g. GMRES)		$O(M^3)$	
MVP	$\mathbf{Z}^{\mathbf{S},\mathbf{S}}\cdot\mathbf{I}^{\mathbf{S}}$	$\mathbf{Z}^{\mathbf{S},\partial\mathbf{S}}\cdot\mathbf{I}^{\partial\mathbf{S}}$,$\mathbf{Z}^{\partial\mathbf{S},\mathbf{S}}\cdot\mathbf{I}^{\mathbf{S}}$	$\mathbf{Z}^{\partial\mathbf{S},\partial\mathbf{S}}\cdot\mathbf{I}^{\partial\mathbf{S}}$
Direct [25]	$O(M^4)$	$O(M^3)$	$O(M^2)$
FMM aided [6]	$O(M^2)$	$O(M^2)+O(M^2)$	$O(M\log M)$
FFT aided [6]			$O(M^2)$
LU-solve	$O(M^6)$	$O(M^3)$	$O(M^3)$
Calculating the E-field inside S			
LU, Iterative	Available directly	$O(M^3)$	$O(M^3)$
FMM, FFT aided		$O(M^2)$	$O(M^2)$
Required Memory without Calculation of the E-field inside of S			
LU, Iterative	$O(M^4)$	$O(M^3)$	$O(M^2)$
FMM aided [6]	$O(M^2)$	$O(M^2)$	$O(M\log M)$
FFT aided [6]			$O(M^2)$
Required Memory with Calculation of the E-field inside of S			
LU, Iterative	$O(M^4)$	$O(M^3)$	$O(M^3)$
FMM, FFT aided	$O(M^2)$	$O(M^2)$	$O(M^2)$

D. Matrix Form of MoM Discretized SVS-EFIE

The MoM discretization of the integral operators $\mathtt{T}_{\epsilon}^{S,\partial S}$, $\mathtt{T}_{0}^{\partial S,S}$, and $\mathtt{T}_{\epsilon}^{\partial S,\partial S}$ in the SVS-EFIE (13) produces corresponding matrix relations (22), (27), and (30). As a result, the SVS-EFIE is reduced to the following set of linear algebraic equations with respect to the $(M\times 1)$ vector of unknown coefficients $\mathbf{I}$ in the expansion of the auxiliary surface current density (20):

$$\left(\mathbf{Z}_{\epsilon}^{\partial S,\partial S}+\mathbf{Z}_{0}^{\partial S,S}\cdot\mathbf{Z}_{\epsilon}^{S,\partial S}\right)\cdot\mathbf{I}=\mathbf{V}. \tag{33}$$

The depiction of the matrix form (33) of the SVS-EFIE (13) is shown in Fig. 2 for the pair of dielectric cylinders in Fig. 1. The above matrix equation (33) can be solved either directly via LU decomposition [25] or iteratively using GMRES [29] or conjugate gradient (CG) [30] algorithms. In case of the iterative solution, the matrix-vector products (MVPs) pertinent to (33) can be accelerated via the fast multipole method (FMM) [31] or the fast Fourier transform (FFT)-based methods [32], [33]. The comparison of the computational complexity of different algorithms is given in Table I. Computational time and memory requirements are described as a function of the number of unknowns M on the surface of the scatterer with the assumption that the cross section is discretized with M^2 elements.

It is important to note that upon acceleration of the matrix-vector multiplies using FFT-based methods [32], [33], the proposed SVS-EFIE solution exhibits the same $O(M^2)$ computational complexity as the solution of the traditional surface IEs [9], [10]. In the traditional surface IE solutions, the $O(M^2)$ complexity arises due to the usage of 2-D FFT operations with the majority of 2-D FFT grid samples populated with zeros due to the localization of the unknown currents on the scatterer's surface [6]. In the proposed method, the $O(M^2)$ complexity arises naturally due to surface-to-volume and volume-to-surface field translations. The proposed SVS-EFIE features the same computational complexity as the traditional surface IEs if the field inside the scatterer is calculated. Moreover, the field inside obtained via SVS-EFIE is less expensive to compute because it requires only M matrix vector products, since the matrix $\mathbf{Z}_{\epsilon}^{S,\partial S}$ associated with the surface-to-volume operator $\mathtt{T}_{\epsilon}^{S,\partial S}$ is already calculated, and does not involve computationally expensive operations.

IV. NUMERICAL STUDIES

Numerical studies for the magneto-quasi-static solution using the proposed SVS-EFIE were considered in detail in our prior publications [19], [20]. In [19], the MoM solution of the SVS-EFIE was compared against the analytic solution for the current flow in a homogeneous conductor of a circular cross section at low, intermediate, and high frequencies. The other numerical examples include the MoM solutions for the single and multiple transmission line configurations with arbitrary cross sections. This includes the coaxial cable transmission line, which features a cross section with the topological multi-connectedness [20].

In this work, we present numerical studies related to the electrodynamic formulation of the proposed SVS-EFIE. In the first numerical experiment, we consider TM_z plane wave scattering from a single dielectric cylinder with the relative permittivity $\varepsilon=11$, as shown in Fig. 3. The cylinder has a circular cross section of the radius $\rho_0=25$ mm. The plane wave of the frequency $f=2$ GHz and of electric field magnitude 1.0 V/m impinges on the cylinder at a 45° angle. The surface current density $\mathtt{J}_z$ is first obtained via the MoM solution (33) of the proposed SVS-EFIE (13) under the uniform discretization of the conductor surface with $M=100$ linear segments and its volume with $N=7\,450$ triangular elements. In order to evaluate the electric field $E_z^{(1)}$ inside the cylinder cross section, the auxiliary current $\mathtt{J}_z$ is substituted into (12). In Fig. 3, the E-field evaluated via the proposed SVS-EFIE (13) and the E-field from the classic PMCHWT solution [10] are compared against the traditional volumetric MoM solution of the V-EFIE (11). The field outside the dielectric body $E_z^{(2)}$ is calculated in two steps. First, the field in the volume of the scatterer is calculated using the single-layer ansatz relation (12). Second, the volumetric distribution of the field inside the scatterer is substituted into the volume equivalence principle to calculate the field outside. The relative error of the proposed SVS-EFIE solution with respect to the MoM solution of the volumetric IE (11) does not exceed 3.2% and has the mean of 0.136% and the standard deviation of 0.116%. In case of the PMCHWT solution, the relative error is bound by 3.3%, has the mean of 0.139%, and the standard deviation of 0.198%.

The equivalent electric current density J_z^e and magnetic current density J_t^m are also found with the MoM solution of the PMCHWT surface IE [10] on the same surface mesh. In Fig. 4, the current densities for both methods are shown along the surface of the cylinder's cross section. From visual comparison in Fig. 4 of the equivalent electric and magnetic current densities J_z^e, J_t^m against the auxiliary surface current density $\mathtt{J}_z$ from the

$$\left(\mathbf{Z}_{\epsilon}^{\partial S,\partial S} + \mathbf{Z}_{0}^{\partial S,S} \cdot \mathbf{Z}_{\epsilon}^{S,\partial S} \right) \cdot \mathbf{I}$$

$$\begin{matrix} & M_A & M_B \\ M_A & \mathbf{Z}_{\epsilon}^{\partial S_A,\partial S_A} & \mathbf{0} \\ M_B & \mathbf{0} & \mathbf{Z}_{\epsilon}^{\partial S_B,\partial S_B} \end{matrix}_{M} + \begin{matrix} & N_A & N_B \\ M_A & \mathbf{Z}_{0}^{\partial S_A,S_A} & \mathbf{Z}_{0}^{\partial S_A,S_B} \\ M_B & \mathbf{Z}_{0}^{\partial S_B,S_A} & \mathbf{Z}_{0}^{\partial S_B,S_B} \end{matrix}_{N} \cdot \begin{matrix} & M_A & M_B \\ N_A & \mathbf{Z}_{\epsilon}^{S_A,\partial S_A} & \mathbf{0} \\ N_B & \mathbf{0} & \mathbf{Z}_{\epsilon}^{S_B,\partial S_B} \end{matrix}_{M} \cdot \begin{matrix} \mathbf{I}^A \\ \mathbf{I}^B \end{matrix}_{M}$$

Fig. 2. Matrix form (33) of the SVS-EFIE (13) discretized with the MoM utilizing depicted in Fig. 1 volume and surface meshes.

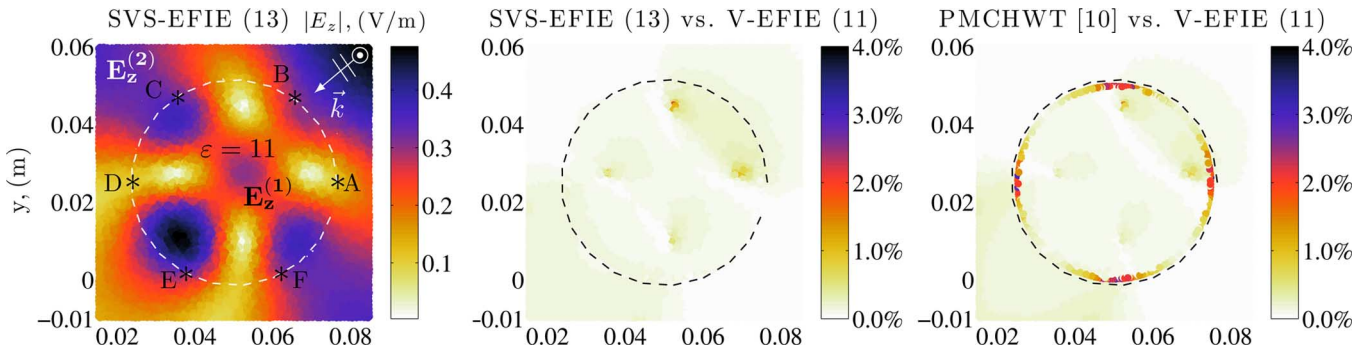

Fig. 3. Distribution of the electric field inside $E_z^{(1)}$ and outside $E_z^{(2)}$ the dielectric cylinder obtained via MoM solution (33). The relative error of the latter (center plot) and the MoM solution of the PMCHWT surface IE solution (right plot) with respect to the volumetric MoM solution of the V-EFIE (11). Points A–F correspond to the points in Fig. 4.

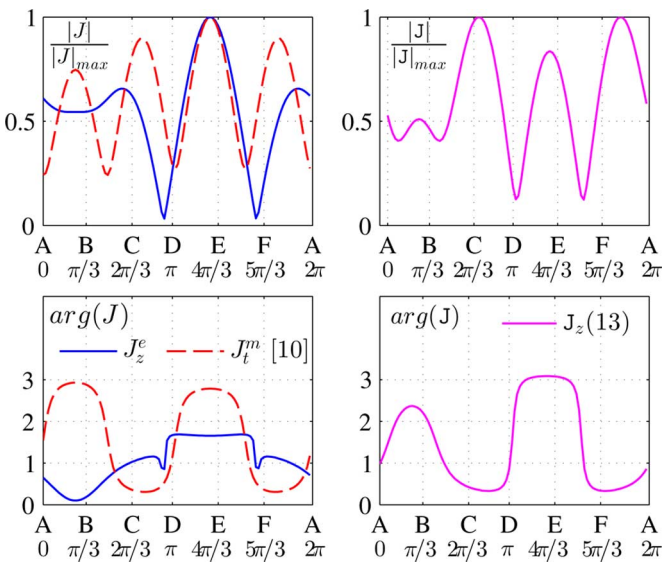

Fig. 4. Equivalent electric and magnetic surface current densities (J_z^e, J_t^m on the left) obtained with the MoM solution of PMCHWT surface IE and the auxiliary surface current density (J_z on the right) obtained with the MoM solution of the proposed SVS-EFIE (13) for TM_z wave scattering from a single dielectric cylinder. Points A–F correspond to the points in Fig. 3.

SVS-EFIE, it is clear that the latter has no apparent relationship to either J_z^e or J_t^m. The auxiliary current J_z is not a superposition of J_z^e and J_t^m. This becomes obvious from J_z behavior for the geometries featuring prominent geometric singularities in the cross section for which J_z remains a continuous function along the surface including the corner points where J_z^e, for example, becomes discontinuous.

The execution time and memory consumption for this experiment are shown in Table II. The results were obtained for a Mathcad worksheet on a single Intel Core 2 Duo processor running at 2.4 GHz. All MVPs were computed directly without using FMM- or FFT-based accelerators [6]. The solution for the field inside the dielectric cylinder was calculated for three meshes via the MoM solution of the V-EFIE (11), PMCHWT [10], and proposed SVS-EFIE (13). The execution time and memory consumtion for the case of the MoM solution of the V-EFIE for the 7460-element mesh is projected from the data for the 1890-element mesh according to the computational complexity of the operations. The behavior of the execution time and memory consumption data reflects the computational complexity analysis results from the previous section. The novel SVS-EFIE is faster than the V-EFIE at all steps and allows to compute the field inside the scatterer at the lower price than in case of the MoM solution of the PMCHWT surface IE.

Next, to demonstrate the error behavior of the proposed SVS-EFIE (13) solution upon the h-refinement [18] of the MoM's surface and volume meshes, the cross section of the hexagonal dielectric cylinder is discretized with the meshes featuring from 48 to 120 line segments and from 1000 to 3719 surface triangles. The mean and standard deviation of the relative error with

TABLE II
COMPUTATIONAL TIME AND MEMORY FOR THE SOLUTION OF THE V-EFIE, SVS-EFIE, AND PMCHWT EQUATIONS IN MATHCAD

	V-EFIE (11)	PMCHWT [10]	SVS-EFIE (13)
M = 10 linear elements, N = 278 triangular elements			
Total Time	**229.5 s**	**2.4 s**	**1.0 s**
Fill Time	228.9 s	0.5 s	0.9 s
Solve Time	0.7 s	≈ 0.1 s	≈ 0.1 s
Field in S	—	1.9 s	≈ 0.1 s
Memory	**13 Mb**	**≈ 1 Mb**	**≈ 1 Mb**
M = 20, N = 1,890			
Total Time	**≈ 4 hrs**	**26.3 s**	**8.8 s**
Fill Time	≈ 4 hrs	1.6 s	8.7 s
Solve Time	28.7 s	≈ 0.1 s	≈ 0.1 s
Field in S	—	24.7 s	≈ 0.1 s
Memory	**147 Mb**	**4 Mb**	**12 Mb**
M = 100, N = 7,450			
Total Time	*2.5 days (projected)*	**245.9 s**	**80.8 s**
Fill Time	*2.5 days*	8.2 s	80.5 s
Solve Time	*7.5 m*	0.1 s	0.1 s
Field in S	—	237.7 s	0.2 s
Memory	*2 Gb*	**40 Mb**	**82 Mb**

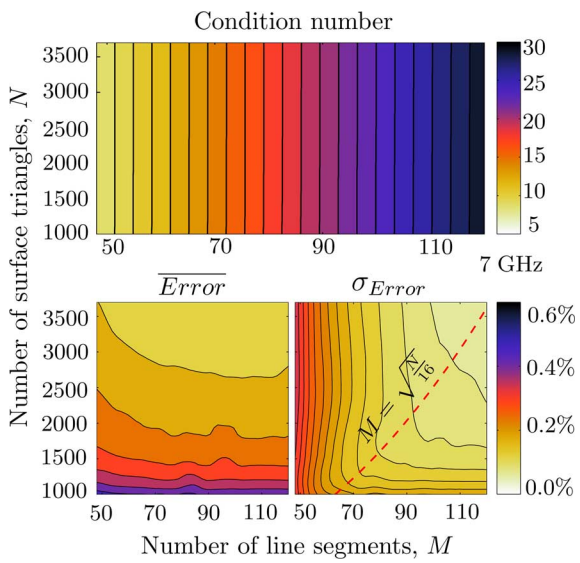

Fig. 5. Condition number of the matrix (33), mean and standard deviation of the relative error of the cross-sectional distribution of the E-field inside the dielectric cylinder obtained via MoM solution (33) with respect to the volumetric MoM solution of the V-EFIE (11) as a function of surface and volume mesh refinement. Optimal volume/surface elements ratio $M = \sqrt{N/16}$.

respect to the volumetric MoM solution of the V-EFIE (11), as well as the condition number with respect to the L2-norm, are depicted in Fig. 5. The condition number of the resultant matrix for the frequency $f = 7$ GHz is small and weakly depends on the number of surface triangles in the mesh. The behavior of the condition number for the low-frequency $f = 100$ MHz is similar with variation of the condition number from 130 to 330 for the same set of the surface and volume meshes. It is also seen that the mean value of the relative error is not dependent of the number of surface elements and remains at the same level for a

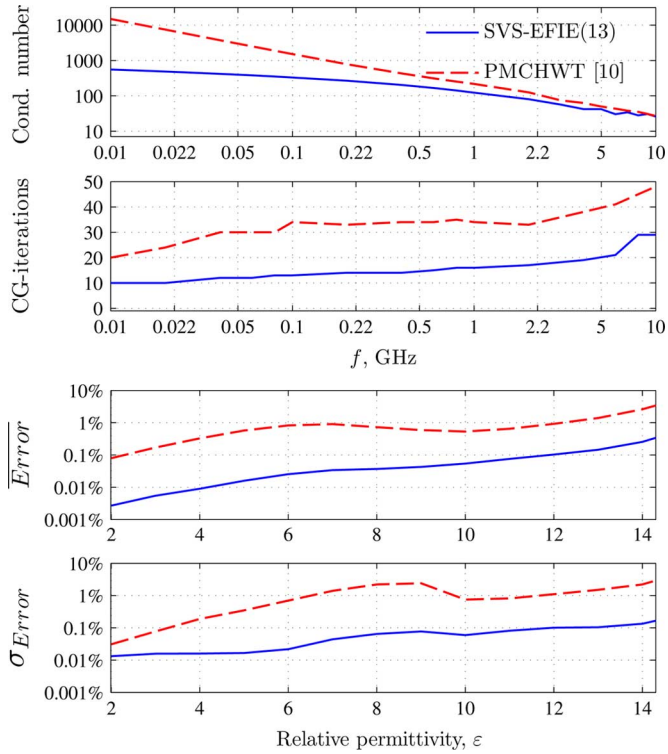

Fig. 6. Condition number of the matrix (33) and impedance matrix for PMCHWT [10] surface IE, required number of CG terations, mean value, and standard deviation of the relative error of the MoM solutions (33) and PMCHWT surface IE for six-sided polygonal approximation of the circular cross section with radius $\rho_0 = 25$ mm due to plane-wave incidence at 2 GHz.

fixed number of volume elements. The optimum number of surface elements M, however, is proportional to the square root of the number of volume elements N as seen from the plot of the standard deviation in Fig. 5. For the particular case of the TM_z scattering from the dielectric cylinder with the relative permittivity $\varepsilon = 2$ and the incident plane wave of frequency $f = 7$ GHz the optimum values of M lie near the curve $M = \sqrt{N/16}$. The same Fig. 5 demonstrates the error-controllable properties of the MoM discretized SVS-EFIE. The latter numerically corroborates the rigorous nature of the proposed SVS-EFIE.

The relative error, condition number, and the number of CG iterations [30] comparison between the MoM solutions of the proposed SVS-EFIE (13) and PMCHWT surface IE is depicted in Fig. 6 for the relative dielectric permittivity of the cylinder varying from 2 to 14. The MoM solution (33) for all values of permittivity utilizes $M = 120$ linear elements and $N = 3\,719$ triangular elements. The MoM solution of PMCHWT surface IE [10] is found using the same surface mesh (albeit it operates with the twice number of unknowns from J_z^e and J_t^m). The systematic accuracy advantage of the proposed SVS-EFIE (13) against the PMCHWT formulation is apparent for all values of ε in both the mean value and standard deviation of the relative error, as well as the smaller condition number and required number of CG iterations to find the solution for the system of linear equations.

The last study compares the MoM solution of the proposed SVS-EFIE (13) against the traditional volumetric MoM solution of the V-EFIE (11) for TM_z wave scattering from a dielectric shell presented in [23]. Fig. 7 shows the electric field

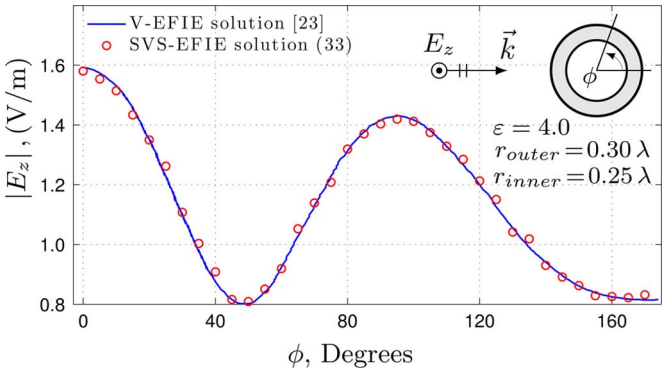

Fig. 7. Electric field distribution in circular dielectric cylindrical shell with plane-wave incident. The MoM solution (33) and numerical results from [23].

distribution inside the dielectric shell due to the incident plane wave of 1.0 V/m magnitude. In this example, the MoM solution (33) of the SVS-EFIE (13) utilizes $M = 80$ linear elements and $N = 520$ triangular elements. A good agreement of the field values is observed with this independent reference solution [23] despite its significantly different MoM discretization of the V-EFIE from the one in this work.

V. Conclusion

The paper has presented a novel rigorous single-source derivative-free surface IE for the problems of determining distribution of volumetric current flow in MTLs and full-wave scattering on homogeneous permeable cylinders. The new surface IE is derived from the classical V-EFIE via the single-layer ansatz representation of the volume current density. It is shown to produce a notably higher accuracy than the standard PMCHWT IE while featuring only a single surface unknown function. This advantage comes at the cost of the field translations performed from surface to volume domains and back unlike the less computationally expensive surface-to-surface field translations in PMCHWT formulation. The new IE does not feature derivatives acting on its kernels, and as such, may be particularly suitable for the analysis in multilayered media.

References

[1] W. C. Chew, *Waves and Field in Inhomogeneous Media*. Piscataway, NJ: IEEE Press, 1995.

[2] J. Morsey, "Integral equation methodologies for the signal integrity analysis of PCB and interconnect structures in layered media from DC to multi-GHz frequencies," Ph.D. dissertation, Dept. Elect. Comput. Eng., Univ. of Illinois at Urbana-Champaign, Urbana-Champaign, IL, 2004.

[3] M. Kamon, M. J. Tsuk, and J. White, "FASTHENRY: A multipole accelerated 3-D inductance extraction program," *IEEE Trans. Microw. Theory Techn.*, vol. 42, no. 9, pp. 1750–1758, Sep. 1994.

[4] B. Young, *Digital Signal Integrity*. New York: McGraw-Hill, 2001.

[5] P. Mojabi and J. LoVetri, "Comparison of TE and TM inversions in the framework of the Gauss–Newton method," *IEEE Trans. Antennas Propag.*, vol. 58, no. 4, pp. 1336–1348, Apr. 2010.

[6] *Fast and Efficient Algorithms in Computational Electromagnetics*, W. C. Chew, J.-M. Jin, E. Michielssen, and J. Song, Eds. Norwood, MA: Artech House, 2001.

[7] S. Cadirci, "RF stealth and counter-RF stealth technologies," M.Sc. thesis, Inf. Sci. Dept., Naval Postgraduate School, Monterey, CA, 2009.

[8] K. Sertel, "Multilevel fast multipole method for modeling permeable structures using conformal finite elements," Ph.D. dissertation, Dept. Elect. Comput. Eng., Univ. Michigan at Ann Arbor, Ann Arbor, MI, 2003.

[9] A. Kishk and L. Shafai, "Different formulations for numerical solutions of single or multibodies of revolution with mixed boundary conditions," *IEEE Trans. Antennas Propag.*, vol. 34, no. 5, pp. 666–673, May 1986.

[10] A. Peterson, S. Ray, and R. Mittra, *Computational Methods for Electromagnetics*. Piscataway, NJ: IEEE Press, 1998.

[11] Z. G. Qian, W. C. Chew, and R. Suaya, "Generalized impedance boundary condition for conductor modeling in surface integral equation," *IEEE Trans. Microw. Theory Techn.*, vol. 55, no. 11, pp. 2354–2364, Nov. 2007.

[12] D. Swatek, "Investigation of single source surface integral equation for electromagnetic wave scattering by dielectric bodies," Ph.D. dissertation, Dept. Elect. Comput. Eng., Univ. Manitoba, Winnipeg, MB, Canada, 1999.

[13] D. R. Swatek and I. R. Ciric, "A recursive single source integral equation analysis for wave scattering by heterogeneous dielectric bodies," *IEEE Trans. Antennas Propag.*, vol. 48, no. 8, pp. 1175–1185, Aug. 2000.

[14] F. Valdes, F. P. Andriulli, H. Bagci, and E. Michielssen, "On the discretization of single source integral equations for analyzing scattering from homogeneous penetrable objects," in *IEEE AP-S Int. Symp.*, Jul. 2008, pp. 1–4.

[15] A. Glisson, "An integral equation for electromagnetic scattering from homogeneous dielectric bodies," *IEEE Trans. Antennas Propag.*, vol. AP-32, no. 2, pp. 173–175, Feb. 1984.

[16] M. S. Yeung, "Single integral equation for electromagnetic scattering by three-dimensional homogeneous dielectric objects," *IEEE Trans. Antennas Propag.*, vol. 47, no. 10, pp. 1615–1622, Oct. 1999.

[17] *Integral Equation Methods in Scattering Theory*, D. Colton and R. Kress, Eds. Malabar, FL: Krieger, 1992.

[18] J.-M. Jin, *The Finite Element Method in Electromagnetics*, 2nd ed. New York: Wiley, 2002.

[19] A. Menshov and V. Okhmatovski, "Novel surface integral equation formulation for accurate broadband *RL* extraction in transmission lines of arbitrary cross-section," in *IEEE MTT-S Int. Microw. Symp. Dig.*, Jun. 17–22, 2012, pp. 1–3.

[20] A. Menshov and V. Okhmatovski, "Method of moment solution of surface–volume–surface electric field integral equation for two-dimensional transmission lines of complex cross-sections," in *IEEE 16th Signal and Power Integrity Workshop*, May 13–16, 2012, pp. 31–34.

[21] *Handbook of Mathematical Functions*, M. Abramovitz and I. Stegun, Eds. New York: Dover, 1964.

[22] F. Ling, "Fast electromagnetic modeling of multilayer microstrip antennas and circuits," Ph.D. dissertation, Dept. Elect. Comput. Eng., Univ. Illinois at Urbana-Champaign, Champaign, IL, 2000.

[23] J. Richmond, "Scattering by a dielectric cylinder of arbitrary cross section shape," *IEEE Trans. Antennas Propag.*, vol. AP-13, no. 3, pp. 334–341, 1965.

[24] R. Harrington, *Field Computation by Moment Methods*. Piscataway, NJ: IEEE Press, 1993.

[25] W. H. Press *et al., Numerical Recipes: The Art of Scientific Computing*. Cambridge, U.K.: Cambridge Univ. Press, 2007.

[26] D. Wilton, A. Glisson, D. Schaubert, O. Al-Bundak, and C. Butler, "Potential integrals for uniform and linear source distributions on polygonal and polyhedral domains," *IEEE Trans. Antennas Propag.*, vol. AP-32, no. 3, pp. 276–281, Mar. 1984.

[27] F. R. Gantmacher, *Matrix Theory*. New York: Chelsea Publishing, 1959.

[28] J. H. Ma, V. Rokhlin, and S. Wandzura, "Generalized Gaussian quadrature rules for systems of arbitrary functions," *SIAM J. Numer. Anal.*, vol. 33, no. 3, pp. 971–996, Jun. 1996.

[29] V. Fraysse, L. Giraud, and S. Gratton, "A set of GMRES routines for real and complex arithmetics," CERFACS, Toulouse, France, CERFACS Tech. Rep. TR/PA/97/49, 2003. [Online]. Available: www.cerfacs.fr

[30] C. H. Smith, A. F. Peterson, and R. Mitra, "The biconjugate gradient method for electromagnetic scattering," *IEEE Trans. Antennas Propag.*, vol. 38, no. 6, pp. 938–940, Jun. 1990.

[31] L. Greengard and V. Rokhlin, "The fast algorithm for particle simulations," *J. Comput. Phys.*, vol. 73, no. 2, pp. 325–348, Dec. 1987.

[32] E. Bleszynski, M. Bleszynski, and T. Jaroszewicz, "AIM: Adaptive integral method for solving large-scale electromagnetic scattering and radiation problems," *Radio Sci.*, vol. 31, no. 5, pp. 1255–1251, Sep. –Oct. 1996.

[33] M. F. Catedra, R. F. Torres, J. Basterrechea, and E. Cago, *The CG-FFT Method: Application of Signal Processing Techniques to Electromagnetics*. Norwood, MA: Artech House, 1995.

Anton Menshov (S'12) was born in Kovrov, Russia, in 1988. He received the B.S. degree in automatics and management from the Moscow Institute of Electronic Technology, Moscow, Russia, in 2010, and is currently working toward the M.Sc. degree in electrical and computer engineering at the University of Manitoba, Winnipeg, MB, Canada. His current research interest are in computational electromagnetics with applications to characterization of MTLs and full-wave scattering problems.

Vladimir I. Okhmatovski (M'99–SM'09) was born in Moscow, Russia, in 1974. He received the M.S. degree (with distinction) in radiophysics and the Candidate of Sciences (Ph.D.) degree in antennas and microwave circuits from the Moscow Power Engineering Institute, Moscow, Russia, in 1996 and 1997, respectively.

In 1997, he joined the Radio Engineering Department, Moscow Power Engineering Institute, as an Assistant Professor. From 1998 to 1999, he was a Post-Doctoral Research Associate with the National Technical University of Athens. From 1999 to 2003, he was a Post-Doctoral Research Associate with the University of Illinois at Urbana-Champaign. From 2003 to 2004, he was with the Department of Custom Integrated Circuits, Cadence Design Systems, as a Senior Member of Technical Staff. In 2004, he joined the Department of Electrical and Computer Engineering, University of Manitoba, Winnipeg, MB, Canada, where is currently an Associate Professor. His research interests are fast algorithms of electromagnetics, high-performance computing, modeling of interconnects, and inverse problems.

Dr. Okhmatovski is a Registered Professional Engineer in the Province of Manitoba, Canada.